# Robust, High-Resolution, Whole Cell Patch-Clamp Capacitance Measurements Using Square Wave Stimulation

Russell E. Thompson, Manfred Lindau, and Watt W. Webb
Cornell University, School of Applied and Engineering Physics, Ithaca, New York 14853 USA

ABSTRACT High-resolution, whole cell capacitance measurements are usually performed using sine wave stimulation using a single frequency or a sum of two frequencies. We present here a high-resolution technique for whole-cell capacitance measurements based on square-wave stimulation. The square wave represents a sum of sinusoidal frequencies at odd harmonics of the base frequency, the amplitude of which is highest for the base frequency and decreases as the frequency increases. The resulting currents can be analyzed by fitting the current relaxations with exponentials, or by a phase-sensitive detector technique. This method provides a resolution undistinguishable from that of single-frequency sine wave stimulation, and allows for clear separation of changes in capacitance, membrane conductance, and access resistance. In addition, it allows for the analysis of more complex equivalent circuits as associated with the presence of narrow fusion pores during degranulation, tracking many equivalent circuit parameters simultaneously. The method is insensitive to changes in the reversal potential, pipette capacitance, or widely varying cell circuit parameters. It thus provides important advantages in terms of robustness for measuring cell capacitances, and allows analysis of complicated changes of the equivalent circuits.

## INTRODUCTION

The plasma membrane of cells appears electrically as a thin insulator separating the cytosol from the exterior bathing solution. It is therefore appropriately modeled as a parallel plate capacitor, with the property that the capacitance is proportional to the membrane area. Thus, membrane capacitance measurements allow a direct detection of changes in membrane area as occurring during the fundamental cellular processes of exocytosis and endocytosis (Neher and Marty, 1982; Fernandez et al., 1984). In addition, it has proved powerful in elucidating details of the membrane fusion process in exocytosis (Breckenridge and Almers, 1987). In combination with other measurements of exocytosis, such as amperometry or fluorescent dye staining, it has provided information on the concentration of neurotransmitter in chromaffin cell granules (Albillos et al., 1997), or the time course of membrane re-uptake after stimulated exocytosis (Smith and Betz, 1996). A good review of the theory and techniques of cell capacitance measurement is given by Lindau (1991) and Gillis (1995).

Most techniques for monitoring whole-cell membrane capacitance work by applying a voltage stimulus via a patch pipette and measuring the resulting currents. Although the initial methods applied a voltage step and analyzed the exponential current decay in the time domain, the most popular methods today are the Lindau–Neher (Lindau and Neher, 1988) and phase-tracking techniques (Fidler and Fernandez, 1989), which both use sinusoidal voltage stimulation and rely on the use of phase-sensitive lock-in amplifier measurements. This change was made largely to take advantage of the high time resolution and sensitivity provided by the sinusoidal stimulation techniques (Neher and Marty, 1982; Lindau and Neher, 1988; Chen and Gillis, 2000). Capacitance measurements using a lock-in amplifier are, however, more sensitive to large conductance changes. To account for large conductance changes, the DC current can be used as an additional quantity (Lindau and Neher, 1988; Gillis, 2000) or two frequency phase-sensitive detector (PSD) techniques can be applied (Rohlicek and Schmidt, 1994; Donnelly, 1994; Barnett and Misler, 1997).

Good noise performance is not unique to the sinusoidal stimulation techniques, but can also be obtained using a square wave stimulation as pointed out by Gillis (1995), and square wave stimulation is quite insensitive to conductance changes (Lindau and Neher, 1988). The historically poor noise performance of square wave techniques is directly due to the low duty cycle of the measurements, caused by discontinuous data acquisition and the long time it took for computers to perform on-line least-squares fitting on the exponential current transients. Typical desktop computers are now fast enough to perform this analysis online, using an optimized algorithm.

A benefit gained by using square wave stimulation is that it provides more information. Single-frequency sinusoidal techniques are essentially limited to measurement of two quantities, the real and imaginary parts of the cell admittance, which is insufficient to determine unambiguously the values of the three components of the cell's minimal equivalent circuit. This becomes significant when large conductance changes occur during an experiment. In the Lindau–Neher technique (Lindau and Neher, 1988), the admittance information is supplemented by assuming a cell-reversal potential and measuring the DC current flowing through the cell, whereas phase tracking (Fidler and Fernandez, 1989) works by dithering the access resistance and imposing the requirement that changes appear only in the real part of the

*Received for publication 20 July 2000 and in final form 7 May 2001.*

Address reprint requests to Watt W. Webb, Cornell University, School of Applied and Engineering Physics, 229 Clark Hall, Ithaca, NY 14853. Tel.: 607-255-3331; Fax: 607-255-7658; E-mail: www2@cornell.edu.



0006-3495/01/08/937/12 $2.00

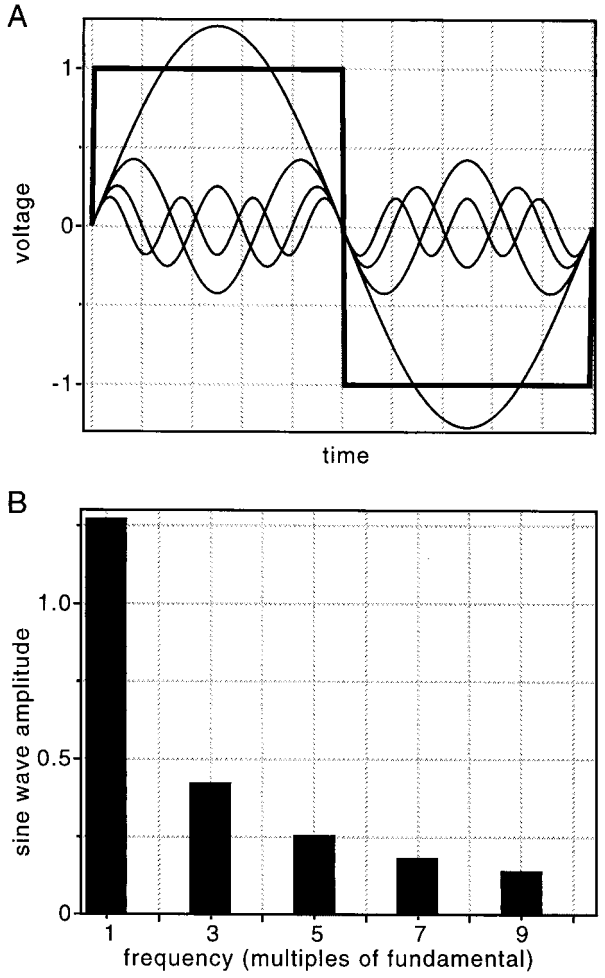


FIGURE 1 A square wave can be decomposed into an infinite sum of sinusoids. (*A*) The first four sinusoidal components of the square wave and the square wave itself. Only odd harmonics of the fundamental are present in the square wave. Note that the amplitude of the first component is larger than the amplitude of the square wave. (*B*) The amplitudes of the sinusoidal components relative to the square wave amplitude as a function of frequency.

admittance. A square wave stimulation, in contrast, can be viewed in the frequency domain as the superposition of a series of odd multiples of the fundamental frequency, with amplitudes decreasing with increasing frequency as shown in Fig. 1. Square wave stimulation thus provides admittance information at a set of frequencies, instead of just one for a single sine wave, or two for two-frequency techniques (Rohlicek and Schmid, 1994; Donnelly, 1994; Barnett and Misler, 1997).

In practice, square wave stimulation proves to be more robust. It works by measuring the amplitude, time constant, and baseline of the exponential current transient, which is sufficient to entirely determine the cell circuit parameters. In addition, the quality of the fit can easily be assayed by measuring how well the current transient conforms to an exponential time course. This can warn of situations when the cell is not well represented by a simple three-component circuit, or, alternatively, can provide extra information when, for example, a fusion pore conductance and vesicle capacitance appear in parallel with the main cell capacitance (Scepek and Lindau, 1993).

Square wave stimulation is insensitive to errors that may arise from reversal potential changes occurring during the experiment, and it can also be made insensitive to errors in pipette capacitance compensation simply by ignoring the current during the time when pipette capacitance transient is active (Lindau and Neher, 1988). The "cap track" method, implemented in the EPC-9 software (Sigworth et al., 1995), is based on square wave stimulation and automatic capacitance compensation adjustment. Dynamic adjustment of the stimulation frequency allows a wide range of cell parameters to be accurately measured. The currents evoked by square wave stimulation can also be analyzed using a phase-sensitive detection technique.

The following sections discuss in detail the insensitivity to pipette capacitance changes, the dynamic adjustment of the stimulus frequency, and the noise performance of the technique. A comparison is made to the frequently used PSD methods, and to methods using two-frequency stimulus waveforms, and the analysis of complex equivalent circuits is explored by fitting the two-component exponential current decays that occur during the fusion of a granule with the plasma membrane. Information necessary to implement the technique is given in the Appendix.

## MATERIALS AND METHODS

### Capacitance measurements

All measurements were made using an EPC-7 patch clamp amplifier connected through a CIO-DAS1601 analog/digital interface card (ComputerBoards, Mansfield, MA) to a Pentium 100-MHz computer. The current signal was filtered using the 10-kHz 3-pole bessel filter of the EPC-7 and acquired at a sampling rate of 50 kHz by the computer. Some of the capacitance noise measurements were made with the EPC-7 10-kHz filter switched off and the current filtered by a Krohn-Hite model 3320 low-pass RC filter set to 20 kHz.

Synchronization of the square wave stimulus voltage to the data acquisition was achieved by triggering an 8243 counter/timer chip (also present on the CIO-DAS1601 interface card) with the analog-to-digital converter (A/D) sampling clock that controlled the current data acquisition. The counter/timer chip was preset to generate a square wave output with an appropriate divisor calculated to set the optimal frequency according to the most recently determined cell circuit parameters (see below). Because the voltage output of the counter/timer was not stable enough to be used directly as a voltage stimulus, the output controlled a DG403 analog switch, which applied alternately either ground or +3.2V (from two AA batteries) to the stimulus input of the EPC-7, creating a ±16-mV square wave at the pipette. The current data acquired by the computer were analyzed online by optionally averaging a number of consecutive cycles and then passing the result to a fast fitting routine as described in the appendix.

The computer also checks for a number of error conditions and responds to them. Most commonly, the cell circuit parameters have changed during the experiment to the point where the stimulus frequency is no longer

optimal. A new frequency is then calculated and the counter/timer chip set appropriately. The computer also checks for A/D first-in-first-out buffer overflows, current values beyond the A/D limits (current overload), and cases when the current trace is more appropriately represented by a seal resistance. In the latter case, the computer calculates the seal resistance and outputs a sound with a frequency corresponding to the resistance to aid in forming a giga-seal. All error conditions and circuit-parameter values as well as the average cell voltage and current are time-stamped and recorded to a log file. In addition, the raw current values are saved directly to another file for more sophisticated analysis of interesting events. The program (written in C) for acquiring and analyzing the current data is available on request. For more information, contact R. Thompson by email at rt14@cornell.edu.

### Cell culture and recording conditions

Rat basophilic leukemia (RBL-2H3) cells were grown to a monolayer in cell culture flasks in minimal essential medium (GIBCO, Carlsbad, CA) supplemented with 10% newborn calf serum and 10% fetal bovine serum. One day before patching, they were passed into dishes with 200 $\mu$M serotonin added to the media to increase the formation of large granules (Williams et al., 1999). Just before patching, the cells were washed with BSS containing (in mM) 135 NaCl, 5 KCl, 1 $MgCl_2$, 1.8 $CaCl_2$, 20 HEPES, 5 glucose, 0.5% BSA, pH 7.4. A cover of oil (tetradecane) was layered on top of the bath solution to prevent capacitance artifacts due to water creeping up the pipette walls. This technique also has the advantage of preventing osmotic pressure changes caused by bath solution evaporation, and allows the use of very little bath solution (about 100 $\mu$m thick) to lower the noise due to dielectric relaxation in the pipette glass (Levis and Rae, 1998). Cells were warmed to 35°C during the experiments using a Bioptechs Delta-T system (Bioptechs, Butler, PA). The pipette solution used was (in mM) 145 K-glutamate, 8 NaCl, 1 $MgCl_2$, 10 NaOH, 10 HEPES, pH 7.2 with KOH. Cells were stimulated to secrete by adding 10 mM ATP and 1.2 mM $CaCl_2$ (De Matteis et al., 1991) to the pipette solution. This was calculated to give 10 $\mu$M free $Ca^{2+}$ using the program MaxChelator (http://www.stanford.edu/~cpatton/maxc.html). Typical pipette resistances were ~4 MΩ. The holding potential was near 0 mV in all experiments.

## RESULTS AND DISCUSSION

Figure 2 shows the equivalent circuit used to model the cell–pipette system, composed of the cell membrane capacitance $C_m$ and conductance $G_m$, and the access conductance at the tip of the pipette $G_a$. The current response to a square wave voltage stimulus consists of two decaying exponentials. Fitting the current response results in an amplitude, time constant, and baseline for each decaying exponential, which can, in turn, be used to calculate the membrane capacitance $C_m$ and conductance $G_m$ and access conductance $G_a$ as described in more detail in the Appendix.

The onset of each exponential transient is rounded due to filtering of the current response by the patch clamp amplifier or other filters. For this reason, and to avoid the effects of the pipette capacitance $C_p$, only the region of the decaying exponentials marked in black is used in the fit (Lindau and Neher, 1988). The filtering also causes a variable delay in the exponentials, which must be compensated for in a calibration procedure. In addition, achieving low measurement noise is critically dependent on the frequency of the voltage stimulus (Lindau and Neher, 1988; Gillis, 1995).

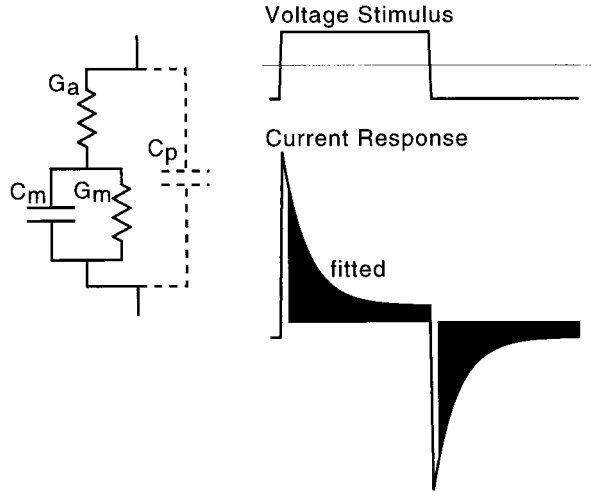


FIGURE 2 The equivalent circuit used to model the cell–pipette system. The cell is represented by the membrane capacitance and conductance $C_m$ and $G_m$. The access conductance $G_a$ occurs at the tip of the patch pipette, and the pipette capacitance $C_p$ (*dashed lines*) represents the various parasitic capacitances between the pipette and bath solution. The currents due to the pipette capacitance are nearly eliminated if correctly compensated with the patch clamp amplifier. A square wave voltage stimulation produces a pair of decaying exponential currents that are each fit using a least-squares technique to yield amplitudes, time constants, and baselines. From the fitted parameters, the cell membrane capacitance and conductance and the access conductance can be determined.

### Insensitivity to changes in $C_p$

The pipette capacitance $C_p$ represents a fourth circuit element that includes all the stray capacitances that occur between the pipette and the bath, as shown in Fig. 2. Most patch clamp amplifiers have a $C_p$ compensation adjustment that allows the user to cancel out most of the current transient due to the pipette capacitance. All of the frequency-domain methods of cell-capacitance measurement require that this cancellation be performed to obtain accurate absolute values for the cell capacitance. Measurements of only relative changes in admittance are still sensitive to $C_p$ changes during the experiment, as can happen if the fluid level in the bath changes due to perfusion, for example. Even if correctly compensated, the pipette capacitance $C_p$ can cause errors in the phase determined through the series resistance dithering technique (Debus et al., 1995, Gillis, 1995).

In a time-domain analysis, in contrast, the $C_p$ transient is generally much shorter than the whole-cell current transient, with a width determined by the low pass filter of the patch clamp amplifier. A good discrimination against the effects of $C_p$ can thus be obtained simply by ignoring the initial section of current containing the $C_p$ transient (Lindau and

Neher, 1988). Using the 10-kHz low-pass filter of the EPC-7 gives a width for the $C_p$ transient of about 40 $\mu$s. Ignoring the first three samples (60 $\mu$s) of each current trace thus provides discrimination against most of the current in the $C_p$ transient. To quantitatively assess the robustness of the method with respect to its insensitivity to changes of stray capacitance or misalignment of C-fast compensation, we used the capacitance compensation circuitry of the EPC-7 amplifier. The C-slow compensation was set to 20 pF with $G_a = 0.1$ $\mu$S to simulate a typical rat basophilic leukemia (RBL) cell. When the C-fast compensation was varied by 1 pF, any changes in the $C_m$ trace were $<0.03$ pF.

The choice of how large a region to ignore is a trade-off between insensitivity to $C_p$ errors and low measurement noise. As more of the trace is discarded, the measurement becomes less sensitive to $C_p$, but the noise is increased because the current in the discarded region represents wasted information (see the section on Noise Performance). Alternatively, we implemented a feature to integrate the current in the rising phase of the transient and added it to the charge under the fitted portion of the transient (see Appendix for details). This procedure greatly decreased the noise for small cells, but gave up the insensitivity to the $C_p$ errors. A third solution is to filter the current signal at a higher bandwidth, which both decreases the measurement noise and heightens $C_p$ insensitivity at the expense of requiring a faster A/D card and computer (see Noise Performance). This becomes important for small cells, but is not critical for cells with $C_m > 10$ pF as used here. Because the raw currents are stored, various methods may be tried in the analysis allowing the optimization of the analysis approach for each individual experiment.

## Dynamic adjustment of stimulus frequency

As shown previously, the optimal frequency for whole cell capacitance measurements using a sine wave stimulus depends on the equivalent circuit parameters (Lindau and Neher, 1988; Gillis, 1995). With our method, the divider in the counter/timer circuit that produces the square wave frequency is under direct computer control, and hence it is easy to add a feedback loop into the capacitance measurement program to adjust the stimulus rate as the cell circuit parameters change. Such a feedback mechanism in the stimulus frequency allows a wide range of circuit parameters over which the measurement will produce precise values. It was found empirically (see Noise Performance) that allowing the current transients to decay over six time constants produced the lowest noise in the capacitance measurement. This criterion was chosen for determining the optimal stimulus frequency.

In Fig. 3, the capacitance compensation controls of the EPC-7 were used to simulate a cell with a constant capacitance of 20 pF and an access resistance varying from 2 to 100 M$\Omega$. The measured cell capacitance $C_m$, in contrast, changed by only 1% over this range. It is likely that a higher order polynomial fit in the calibration procedure (see Appendix) would reduce this deviation even further.

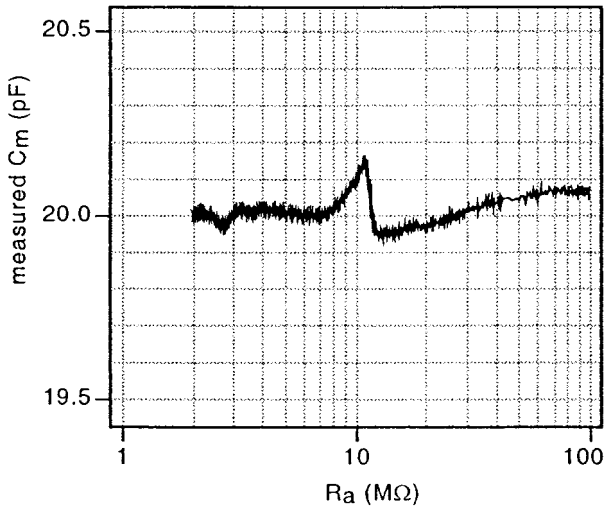


FIGURE 3 The measured membrane capacitance deviates by only 1% as the access resistance is changed over almost two orders of magnitude. The capacitance compensation controls of the patch clamp amplifier were used to simulate a cell.

The technique can thus provide accurate capacitance data over a wide range of access conductances, allowing useful data to be obtained even in experiments in which the pipette tip becomes clogged. In contrast, a low access resistance is often desirable to obtain low noise data, or to adequately fill the cell with a diffusible substance from the pipette.

## Insensitivity to $G_m$ changes

The ability of a technique to cleanly separate changes in $C_m$, $G_m$, and $G_a$ is a major criterion of its usefulness. Figure 4 shows an example of a recording with changes in $C_m$, $G_m$, $G_a$, and the whole cell current $I$. The current trace shows slow fluctuations that are mirrored in the $G_m$ trace, as expected for true changes in $G_m$. In contrast, no corresponding fluctuations are apparent in the traces for $G_a$ and $C_m$. Accordingly, the smooth increase in $G_a$ and the stepwise changes in $C_m$ show no corresponding phenomena in the $G_m$ trace. Transient spikes in the $G_m$ and $G_a$ traces are associated with the two largest capacitance steps. These are due to transient narrow fusion pores with low conductance. As discussed in more detail in Analysis of Complex Equivalent Circuits, the equivalent circuit of Fig. 2 is insufficient at these moments to describe properly the electrical properties of the cell.

Large conductance changes have been the most challenging complication in patch-clamp capacitance measurements. The Lindau–Neher technique allows correction for these, provided that the reversal potential is known with sufficient accuracy (Lindau and Neher, 1988). This method has re-

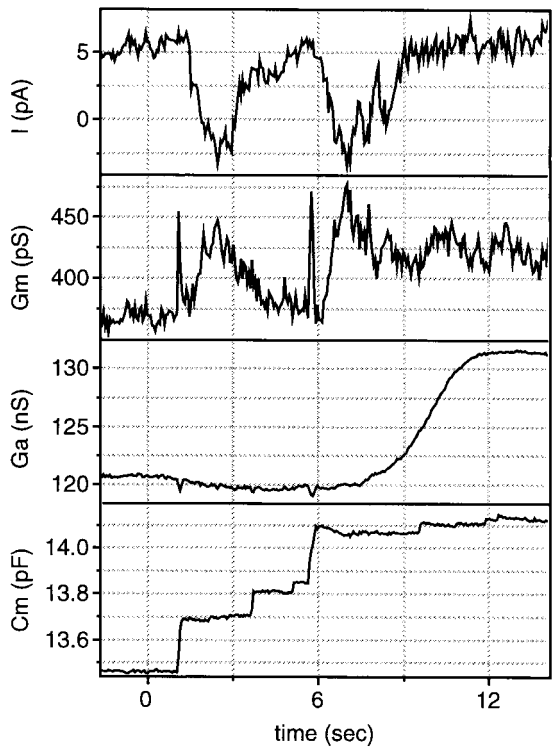


FIGURE 4 A sample capacitance recording from an RBL-2H3 cell demonstrating a clean separation of the cell capacitance $C_m$, membrane conductance $G_m$, access conductance $G_a$, and whole cell current $I$. Steps in capacitance, increases in access conductance, and transient membrane current flows can occur with no significant influence on the other traces.

cently also been implemented in the computer-controlled EPC-9 amplifier (Gillis, 2000). Other schemes use two-frequency PSD techniques (Rohlicek and Schmidt, 1994; Donnelly, 1994; Barnett and Misler, 1997). Time-domain methods are able to cleanly separate large changes in the three elements of the equivalent circuit of Fig. 2 (Lindau and Neher, 1988; Sigworth et al., 1995). With the continuous square wave method described here, high $G_m$ manifests itself as a larger gap between the baselines at the two potentials of the square wave. To obtain an unbiased estimate of membrane conductance, the parameters of the least squares fit (Eq. 5) are used to determine $G_m$ using Eqs. A29 and A30 (see Appendix).

## Noise performance

Traditionally, capacitance measurements using square wave stimulation have yielded low-resolution, noisy results. This is, however, not intrinsic to the method, but rather a reflection of the low duty cycle previously used in these measurements. If the stimulus repetition rate, or frequency, is increased to eliminate the dead time when no information is being acquired, then the noise performance becomes similar to that of the high-resolution sinusoidal stimulation techniques.

The major limitation to increasing the repetition rate is in the on-line computerized fitting of the exponential current decays. We have optimized the least-squares fitting algorithm to run at approximately 100 Hz on a Pentium 100 MHz computer. This provides appropriate time resolution for the majority of experiments (Lindau, 1991), while the maximum bandwidth can be obtained for interesting regions by offline fitting of the saved current transients, or by the use of a faster computer.

To minimize the measurement noise, the time between pulses should be short enough to minimize the dead time when no information is being acquired, but long enough to be able to see significant curvature in the exponential decay from which the time constant can be measured. Because the time constant $\tau$ of the exponential decay is the only variable with the same dimension as the stimulus period, we expect that the noise in the capacitance measurement should be a function of $t_{period}/\tau$. Optimal measurements should be obtained by keeping the stimulus period $t_{period}$ to be some constant times the measured $\tau$. We determined this constant empirically to be approximately 12, giving 6 time constants for the decay of each exponential.

It is interesting to note that the stimulus frequency derived according to this criterion is similar to the optimal frequency for PSD measurements as derived by Gillis (1995). Minimizing the rms $C_m$ noise (Eq. 51 of Gillis, 1995) using a typical ratio of $G_a/G_m = 100$ results in an optimal frequency of $f \approx G_a/20C_m$, or a period of about 20 time constants. The equation thus gives frequencies close to those used here.

Figure 5 shows the measured capacitance noise for a variety of model cells with capacitances from 5 to 33 pF and an access resistance of 5.6 MΩ. Measurements were made with filtering either at 10 or 20 kHz, and either ignoring or integrating the rising phase of the transient and adding the charge to the result of the least squares fit (extra integration) as described in more detail in the Appendix. We used the formula,

$$\frac{\Delta C}{C} = \frac{(4kTR_aB)^{1/2}}{U} \quad (1)$$

(Gillis, 1995), to calculate the theoretical minimum noise for a single-frequency sine wave, where $\Delta C/C$ is the relative capacitance noise, $kT$ is the thermal energy at recording temperature, $R_a = 1/G_a$ is the access resistance, $B$ is the bandwidth, and $U$ is the sine wave amplitude. This formula assumes sinusoidal stimulation at an optimum frequency and that the Johnson noise of the resistor is the only noise source. The noise bandwidth equals the number of measurements per second, and is obtained as $B = f/m$, where $f$ is the square frequency and $m$ is the number of cycles averaged for each data point (Gillis 1995). Because the square wave frequency is changed depending on the time constant of the model cell, the measurement bandwidth varied for the different model

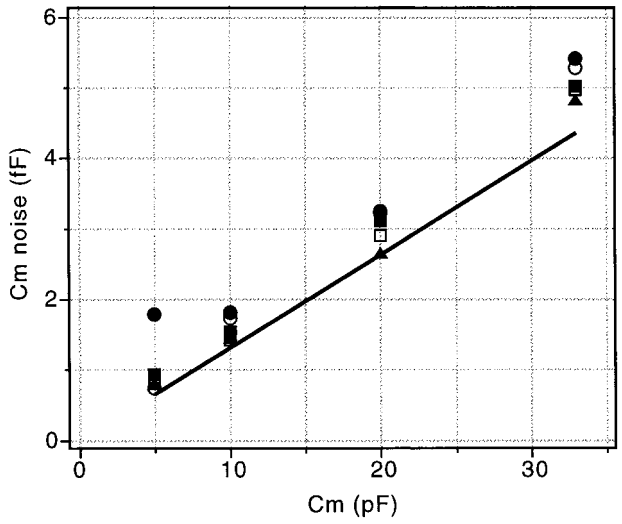


FIGURE 5 Capacitance noise measurements for the least-squares fitting technique under a variety of conditions. Measurements were taken with low-pass filtering of 10 kHz (*circles*), or 20 kHz (*squares*), either ignoring the current data in the $C_p$ transient region (*closed symbols*) or performing an extra integration of that current (*open symbols*). In addition, the 10-kHz data were reanalyzed using a software PSD (*triangles*). For comparison, the theoretical prediction of Eq. 1 is shown assuming a sine wave amplitude of 16 mV (*straight line*). Model cells used had capacitances of 5 to 33 pF and an access resistance of 5.6 MΩ. Measurements were taken with a square wave of ±16 mV and are adjusted to a bandwidth of 50 Hz as described in the text.

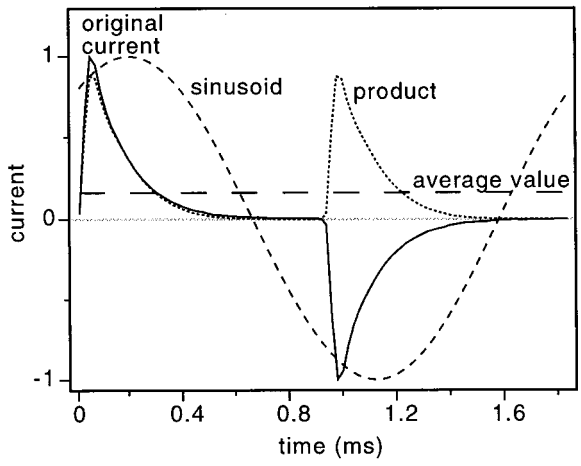


FIGURE 6 An illustration of a PSD analysis on the currents deriving from a square wave voltage stimulation. The original current (*solid line*) is multiplied by a sine wave or cosine wave (*short-dashed line*) to produce a product (*dotted line*) that is then averaged over a complete cycle (*long-dashed line*). The averages give the real and imaginary components of the current at the fundamental frequency. The appropriate phase that reflects the cell membrane conductance and capacitance is calculated using the values for $C_m$ and $G_a$ derived from a least-squares fit.

cells. To compare noise values at the same time resolution, the noise values were adjusted as

$$\Delta C_{\text{displayed}} = \left(\frac{50\text{Hz}}{B}\right)^{1/2} \Delta C_{\text{measured}},$$

where $B$ is the measurement bandwidth.

In measurements using a sinusoid, the capacitance noise $\Delta C$ should increase linearly with $C$ such that the relative capacitance noise $\Delta C/C$ is constant (Eq. 1). The capacitance noise calculated from Eq. 1 is plotted as a straight line in Fig. 5, assuming an access resistance $R_a = 5.6$ MΩ, a bandwidth $B_N = 50$ Hz, and a sine wave amplitude of 16 mV. The measurements for model cells with $C_m > 10$ pF are very close to the theoretical limit as previously found for sinusoidal PSD measurements (Gillis, 1995). For very small cells, ignoring the part containing possible contributions from $C_p$ becomes a severe limitation at 10 kHz filtering. This can be overcome by extra integration of the rising phase or by filtering at a higher frequency. At 20 kHz, the noise is again close to the theoretical limit, although also with this setting, further improvement is obtained by the extra integration.

Increasing the filtering frequency from 10 to 20 kHz lowered the capacitance noise by shortening the time consumed by the rising phase of the transient and hence decreasing the fraction of charge discarded. An alternative scheme (see Appendix for details) is to integrate the charge in the rising phase and add it back to the charge under the fitted portion of the exponential (extra integration in Fig. 5). This technique prevents the increase in noise seen with small cells at the expense of making the measurement sensitive to the pipette capacitance setting. The ratio of the measured capacitance noise to that predicted by Eq. 1 is ~1.2 for the model cells tested, comparable to sine wave methods (Lindau and Neher, 1988; Gillis, 1995).

The pulse duration also affects the accuracy of the $G_m$ estimate such that longer pulses tend to reduce the noise in the $G_m$ estimates. Depending on the requirements for accuracy in $C_m$ versus $G_m$ in particular experiments, a lower square wave frequency may be chosen if small conductance changes are to be determined precisely at the expense of somewhat reduced resolution of $C_m$.

## Phase-sensitive detector analysis

A square wave can be viewed as the superposition of set of sinusoids at odd harmonics of the fundamental frequency. Square wave stimulation can thus provide admittance information at a set of frequencies. The fundamental provides the same information as is gained through single sinusoid techniques, while the harmonics provide extra information that can be used, for example, to determine the phase setting.

Because a PSD acts essentially as a narrow bandpass filter, it is also possible to discard the higher frequency information and recover the signals that would be obtained in a PSD measurement with a single-frequency sine wave. Figure 6 illustrates the procedure. Real and imaginary parts

of the admittance are calculated by multiplying the measured currents with a sinusoid of the appropriate phase and averaging over each cycle. The phase of the part of the sinusoid sensitive to $C_m$ changes is calculated according to the equation

$$\theta = 2 \arctan(\omega C_m/G_a) \quad (2)$$

(Gillis, 1995), using the values for $\omega$, $C_m$, and $G_a$ derived from the least-squares fit.

The capacitance noise obtained with PSD analysis of the raw current recordings from square wave stimulation was generally somewhat lower than that obtained with exponential fitting (Fig. 5, *triangles*). The amplitude of the fundamental sinusoid contained in the square wave has an amplitude 27% larger than the square wave, and only two parameters are determined with PSD analysis instead of three with the time-domain analysis, which should reduce the noise in PSD analysis. In contrast, the time-domain analysis takes into account information not only from the fundamental sinusoid but also from higher frequencies contained in the square wave. Some of this high frequency information is, however, lost due to low pass filtering and by disregarding the initial portion of the capacitive transient, which contains contributions of $C_p$. If extra integration were performed, misalignment of $C_p$ compensation would deteriorate the quality of the fit. The interplay of these different influences is complex. The particular method of fitting the exponential decay should matter only insofar as to the degree at which the charge in the initial part is included or not and whether it is distorted by incomplete $C_p$ compensation. Otherwise, the particular method should not affect the noise as long as the fits yield the same set of parameters with no significant difference in chi-square.

## Two frequency methods

Two schemes have been proposed that use lock-in detection of two sine waves to provide four measured parameters and hence sufficient information to determine the three circuit parameters (Rohlicek and Schmid, 1994; Donnelly, 1994). Both setups used a 2:1 ratio of frequencies with equal amplitudes, resulting in a sinusoidal amplitude of 60% of the voltage excursion, and used a nonoptimized technique for calculating the three circuit parameters from the four measured parameters. For the same voltage excursion, the two-frequency methods result in somewhat larger noise compared to single-frequency methods (Gillis, 1995) but provide independence of the cell reversal potential and applicability down to membrane resistances as low as 50 MΩ. A third technique with two frequencies used nonlinear least-squares fitting to calculate the circuit parameters and showed reduced noise in comparison to the previous two techniques (Barnett and Misler, 1997).

The square wave stimulation represents a sum of many frequencies, and thus is similar conceptually to the two-frequency methods. The particular summation represented by the square wave is advantageous in that the amplitude of the fundamental sine wave is 127% of the voltage excursion. An increased sinusoidal amplitude directly results in lower noise. The large number of frequencies, in addition, of square wave stimulation potentially provides more than the four measured parameters of the two-frequency methods. Thus, given sufficiently good signal-to-noise, it is possible to fit more complex equivalent circuits, as for example occurs in compound exocytosis in eosinophils (Scepek and Lindau, 1993).

## Analysis of complex equivalent circuits

In addition to calculating the capacitance values immediately using the fast exponential fitting algorithm, the computer saves the raw current data as a series of traces. The raw current data during interesting events can then be re-fit using an alternative circuit model to describe the currents (Scepek and Lindau, 1993), or applying a phase-sensitive detector technique to give the same results as a sinusoidal stimulation method.

We have made use of this feature to analyze further the currents that flow during the fusion of exocytotic granules to the plasma membrane in RBL-2H3 cells loaded with serotonin. Serotonin loading induces the formation of large granules in RBL-2H3 cells (Maiti et al., 1997). During exocytosis events, the equivalent circuit must be expanded by the inclusion of a granule capacitance $C_v$ and fusion pore conductance $G_p$ as shown in Fig. 7 (Breckenridge and Almers, 1987). With this equivalent circuit, a voltage step leads to a current transient with two exponential decay components (Scepek and Lindau, 1993).

Figure 8 *A* shows the fitted parameters versus time during the exocytosis of a large (649 fF) granule, assuming the simple equivalent circuit of Fig. 7. $C_m$, $G_a$, and $G_m$ were determined by least-squares fitting of the saved current traces to a three-component circuit model with the calculated currents smoothed by the experimentally determined impulse response function of the recording apparatus. During the time of the capacitance rise (*top trace*), the membrane conductance $G_m$ (*middle trace*) shows a transient increase. A similar phenomenon has been observed in previous capacitance measurements with a lock-in amplifier and reflects the presence of a narrow fusion pore (Spruce et al., 1990). The transient increase in $G_m$ indicates that the analysis must be expanded to include the granule capacitance $C_v$ and fusion pore conductance $G_p$ in the equivalent circuit of Fig. 7.

Figure 8 *B* shows the result of fits to the five-component circuit. Due to the small amplitude of the second exponential component, fits varying all five parameters were unstable and did not converge. We thus performed fits where $C_m$,

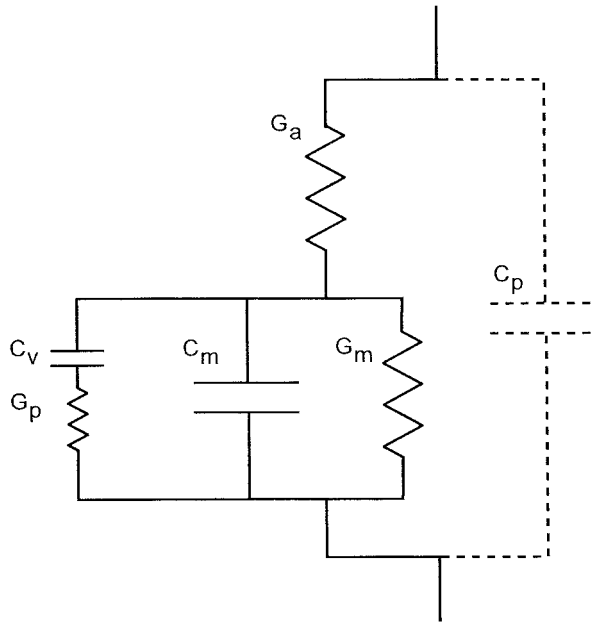


FIGURE 7 The equivalent circuit used for fusion pore analysis. The equivalent circuit as shown in Fig. 2 has been extended by the addition of a series circuit of a granule capacitance $C_v$ and a fusion pore conductance $G_p$ in parallel with the cell membrane. The effect of the additional elements is to add a slowly decaying exponential current to the normal currents seen in response to a voltage step.

$G_a$, and $G_m$ (derived from a three-component fit) were fixed to their values at the beginning of the traces, and $C_v$ was fixed to the difference in $C_m$ from the beginning to the end of the data. Thus, only $G_p$ was allowed to vary in the second stage of fitting. The mean square error of the second stage of fitting (*solid line*) is smaller than the first stage (*dotted line*) during the fusion pore opening (0.4–0.8 s), indicating a better fit in spite of having only one free parameter instead of three.

The effect of opening a small fusion pore is to add a small amplitude, long time-constant exponential to the current transient. The time constant must be, in all cases, longer than the whole-cell time constant, because the vesicle is being charged by the voltage on the cell membrane. This long time constant leads to an apparent increase in the baseline of a three-component exponential fit, which manifests itself as an apparent increase in the membrane conductance $G_m$. The attempt to fit the double exponential with a three-component model also causes an apparent decrease in $G_a$.

In addition to the five-component fit, we implemented an offline PSD technique to analyze the current data. Figure 8 *C* shows a re-analysis of the current transient data with the software-based PSD technique, with a phase of 43.47 degrees calculated using Eq. 2 and the values $\omega = 2380/s$, $C_m = 21.42$ pF, and $G_a = 0.128$ $\mu$S. The changes in the real part Re[$Y$] and imaginary part Im[$Y$] of the conductance

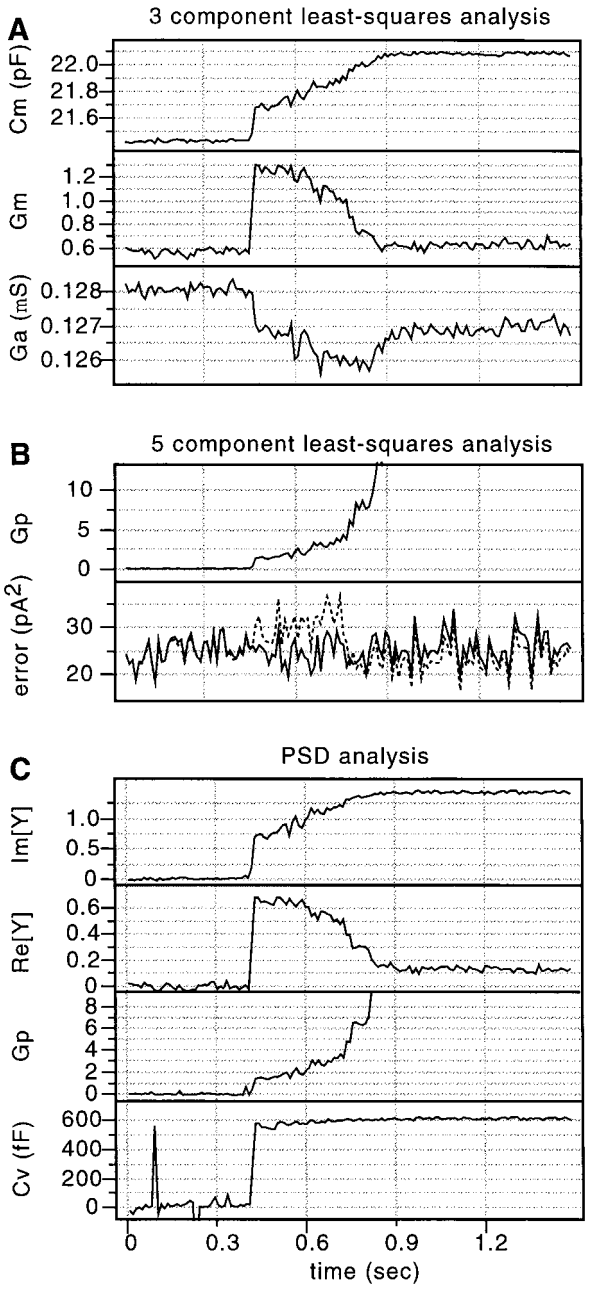


FIGURE 8 Fusion of a large (649 fF) granule during calcium/ATP-stimulated secretion in a serotonin-loaded RBL-2H3 cell. (*A*) Analysis of the current data using the standard three-component equivalent circuit. (*B*) A five-component equivalent circuit was used with the values of $C_m$, $G_a$, $G_m$, and $C_v$ fixed and the fusion pore conductance $G_p$ allowed to vary. (*C*) Analysis of the current data with a software PSD to extract the real and imaginary parts of the conductance and calculate the vesicle capacitance $C_v$ and fusion pore conductance $G_p$ according to the five-component equivalent circuit. The fusion pore appears to open with an initial conductance of ~1 nS. See the text for details on the calculation of the fusion pore conductance $G_p$ by either least-squares fitting or by the software lock-in measurement. All units are nS unless specified otherwise.

roughly correspond to changes in the membrane conductance and membrane capacitance (Lindau, 1991).

The fusion pore conductance $G_p$ and vesicle capacitance $C_v$ were calculated according to the formulas (Lindau, 1991)

$$G_p = \frac{\mathrm{Re}[Y]^2 + \mathrm{Im}[Y]^2}{\mathrm{Re}[Y]}, \quad (3)$$

$$\omega C_v = \frac{\mathrm{Re}[Y]^2 + \mathrm{Im}[Y]^2}{\mathrm{Im}[Y]}. \quad (4)$$

This analysis recovers a clear capacitance step, demonstrating that this event represents fusion of a single granule.

The noise in the membrane capacitance for the pre-fusion event data in Fig. 8 is 17.1 fF for the least-squares fit and 13.5 fF for the PSD analysis, with a bandwidth, in both cases, of 379 Hz. The theoretical noise with the cell parameters that were determined via least-squares fits is 9.9 fF according to Eq. 1. Measurements on actual cells can therefore come close to theoretical predictions and measurements on model circuits (Fig. 5). The results of the PSD analysis (with the phase determined via least-squares fit parameters) and the least squares analysis agree well, with similar time courses and magnitudes of the membrane capacitance, membrane conductance, and fusion pore conductance.

## CONCLUSION

Time-resolved capacitance measurements provide a widely used tool to study the dynamics of exocytosis and endocytosis in single cells and provide a sensitivity that allows one to resolve details of single fusion and fission events. The membrane capacitance and its changes can be obtained in voltage clamp experiments, measuring the currents in response to small voltage steps or by applying a sine wave voltage and analyzing the resulting currents with a phase-sensitive detector or lock-in amplifier (for review see Gillis, 1995; Lindau, 1991). Until now, high-resolution measurements allowing resolution of exocytosis of single vesicles have been performed using single-frequency sine wave stimulation (Fernandez et al., 1984; Neher and Marty, 1982). In the whole-cell patch clamp configuration, the simplest equivalent circuit consists of a parallel combination of membrane capacitance and membrane conductance in series with the access resistance (Hamill et al., 1981; Neher and Marty, 1982). Because measurements using a single frequency provide only two parameters, the amplitude and phase of the current, additional information is required to track all changes independently. The Lindau–Neher technique uses measurement of the DC current (low-pass filtered to remove the sine wave component) to derive all three equivalent circuit parameters (Lindau and Neher, 1988) without compromising the resolution (Gillis, 1995; Chen and Gillis, 2000). This method requires knowledge of the reversal potential of the membrane conductance throughout the recording. Another method is the phase-tracking technique (Fidler and Fernandez, 1989) in which the change in sine wave current in response to switching in a resistor between bath electrode and ground potential, which provides an estimate of the phase at which capacitance changes are expected to be well isolated. This method relies on the assumption that the stray capacitance and membrane conductance are negligible (Debus et al., 1995; Gillis, 1995). Very recently, a system has been described that allows the easy use of the Lindau–Neher technique by automatically calculating the phase delay caused by the patch clamp amplifier for a wide range of instrument settings using the software-controlled EPC-9 patch clamp amplifier (Gillis, 2000).

Other methods have been used that allow the determination of all three parameters of the equivalent circuit simultaneously. These include the use of voltage steps (Gillis, 1995; Lindau, 1991; Lindau and Neher, 1988) or frequency domain transfer function measurements (Clausen and Fernandez, 1981; Fernandez et al., 1984; Joshi and Fernandez, 1988). With these methods, the equivalent circuit parameters can be correctly determined and even much more complicated equivalent circuits can be analyzed (Fernandez et al., 1982; Fishman, 1985). However, these methods sampled the cell in a discontinuous manner and provided low time resolution. High time resolution and independence of reversal potential changes were achieved by superposition of two sine waves with different frequency (Barnett and Misler, 1997; Donelly, 1994; Rohlicek and Rohlicek, 1993; Rohlicek and Schmid, 1994). These methods have not been used very widely. When the same maximal voltage excursion is used, the two-frequency methods have somewhat lower capacitance resolution, and no method has yet been described that allows use of these methods to perform fusion pore analysis. Sigworth et al. (1995) described a method of capacitance measurement (Cap Track) based on square wave stimulation and adjusting the capacitance compensation controls to keep the cell well compensated. Tests of this method reported by Gillis (1995) compared very well to sinusoidal techniques.

The continuous square wave simulation applied here combines advantages from all the various methods described above. The square wave represents superposition of an infinite number of sine waves that are odd multiples of the fundamental frequency, the amplitudes of which decrease as $1/f$. As a result, the total amplitude, the actual voltage excursion, is smaller than the amplitude of the fundamental frequency, which slightly improves the signal-to-noise ratio.

The method thus represents a multifrequency technique providing improved instead of decreased resolution at the optimal frequency used to measure capacitance changes. The currents can be analyzed using a PSD algorithm in just the same way as single-frequency sine wave data. With present

computers, continuous recording of the raw current, on-line analysis, and storage of the raw current for more sophisticated off-line re-analysis has become possible. We have shown how analysis of the currents evoked by voltage steps can be done with various methods, revealing high-resolution records and details of fusion pore opening and expansion.

Time domain and PSD analysis provide complementary results. The time domain analysis provides unambiguous results for $C_m$, $G_m$, and $G_a$. In our hands, the noise of $C_m$ estimates was slightly higher with time-domain than with PSD analysis. This will be more pronounced for very small cells with very fast time constants unless much higher sampling rates are used. However, under those conditions, the time domain analysis may be used to obtain the phase for subsequent PSD analysis, which then provides a resolution as high as single sinusoid measurements. Similarly, for single fusion events of relatively small vesicles, fusion pore analysis probably also requires PSD analysis. The storage of raw current data allows reanalysis, modeling the cell with arbitrarily complicated equivalent circuits. Depending on the signal-to-noise of individual recordings, any type of equivalent circuit can, in principle, be analyzed, provided the number of free (unknown) parameters is kept sufficiently low. We anticipate that even transfer function analysis in the frequency domain might be applied to the stored currents to analyze the equivalent circuit properties and their changes associated with fusion and fission during exocytosis and endocytosis.

## APPENDIX: FITTING METHOD

We use the equivalent circuit shown in Fig. 2 (Joshi and Fernandez, 1988) as a model for the cell–pipette system. The job of the fitting program is then to estimate the circuit parameters from measurements of the transient current responses to the square wave voltage stimulation. It proceeds in two steps. First, each transient current is fit to a decaying exponential function, yielding estimates of the amplitude, time constant, and baseline. Then, pairs of the estimates are used to calculate the membrane capacitance $C_m$, membrane conductance $G_m$, and access conductance $G_a$.

The solution to the least-squares fit of an exponential current decay $y_t$ is defined by the equations

$$0 = \begin{pmatrix} \partial_a \\ \partial_\gamma \\ \partial_b \end{pmatrix} \sum_{t=0}^{N-1} (ae^{-\gamma t} + b - y_t)^2, \tag{A1}$$

where $t$ is in units of the sample spacing. It is necessary to multiply the $\gamma$ found by fitting to this equation by the sample frequency to convert to units of 1/s.

Note that, once the proper decay rate $\gamma$ is found, the Eqs. A1 reduce to a set of linear equations, and the amplitude $a$ and baseline $b$ can be calculated directly. The general three-dimensional minimization problem thus reduces to one dimension. We find $\gamma$ by replacing the variable $\gamma$ with $\gamma = \gamma_0 + \Delta\gamma$ (where $\gamma_0$ is an a priori estimate of $\gamma$), linearizing the three Eqs. A1 around $\gamma_0$, and solving the three equations for $\Delta\gamma$ while eliminating $a$ and $b$. The result is

$$\Delta\gamma = \frac{GH - EF}{E(-2A_2 + B_1^2/N + B_0B_2/N) + FI - GJ - H(-B_2D_0/N + C_2)}, \tag{A2}$$

where we have defined the quantities $E$, $F$, $G$, and $H$ as

$$E = B_0D_0/N - C_0, \tag{A3}$$

$$F = A_1 - B_0B_1/N, \tag{A4}$$

$$G = B_1D_0/N - C_1, \tag{A5}$$

$$H = A_0 - B_0^2/N, \tag{A6}$$

$$I = -B_1D_0/N + C_1, \tag{A7}$$

$$J = -2A_1 + 2B_0B_1/N, \tag{A8}$$

and $A_n$, $B_n$, $C_n$, and $D_n$ as

$$A_n = \sum_{t=0}^{N-1} t^n e^{-2\gamma_0 t}, \tag{A9}$$

$$B_n = \sum_{t=0}^{N-1} t^n e^{-\gamma_0 t}, \tag{A10}$$

$$C_n = \sum_{t=0}^{N-1} y_t t^n e^{-\gamma_0 t}, \tag{A11}$$

$$D_n = \sum_{t=0}^{N-1} y_t^{n+1}. \tag{A12}$$

The summations for $A_n$ and $B_n$ can be solved to give

$$A_0 = \frac{1 - e^{-2\gamma_0 N}}{1 - e^{-2\gamma_0}}, \tag{A13}$$

$$A_1 = -\frac{Ne^{-2\gamma_0 N}}{1 - e^{-2\gamma_0}} + \frac{(1 - e^{-2\gamma_0 N})e^{-2\gamma_0}}{(1 - e^{-2\gamma_0})^2}, \tag{A14}$$

$$A_2 = -\frac{N^2e^{-2\gamma_0 N}}{1 - e^{-2\gamma_0}} + \frac{e^{-2\gamma_0} - (2N + 1)e^{-2\gamma_0(N+1)}}{(1 - e^{-2\gamma_0})^2} + \frac{2(1 - e^{-2\gamma_0 N})e^{-4\gamma_0}}{(1 - e^{-2\gamma_0})^3}, \tag{A15}$$

$$B_0 = \frac{1 - e^{-\gamma_0 N}}{1 - e^{-\gamma_0}}, \tag{A16}$$

$$B_1 = -\frac{Ne^{-\gamma_0 N}}{1-e^{-\gamma_0}} + \frac{(1-e^{-\gamma_0 N})e^{-\gamma_0}}{(1-e^{-\gamma_0})^2}, \quad \text{(A17)}$$

$$B_2 = -\frac{N^2 e^{-\gamma_0 N}}{1-e^{-\gamma_0}} + \frac{e^{-\gamma_0} - (2N+1)e^{-\gamma_0(N+1)}}{(1-e^{-\gamma_0})^2} + \frac{2(1-e^{-\gamma_0 N})e^{-2\gamma_0}}{(1-e^{-\gamma_0})^3}. \quad \text{(A18)}$$

In these equations, the zero point of the time axis is taken to be the beginning of the fitting region, because any time delay is compensated in the process of correcting for the patch clamp filtering circuitry. Because the linearized calculation will not, in general, jump to the correct answer, the calculation is iterated up to ten times using updated estimates of $\gamma_0 = \gamma_0 + \Delta\gamma$. In practice, three iterations were sufficient to converge to a relative accuracy of $\Delta\gamma/\gamma_0 < 10^{-6}$.

After $\gamma$ has been determined, the amplitude $a$, baseline $b$, and sum of squared errors $\chi^2$ can be calculated according to

$$a = -(E + \Delta\gamma I)/(H + \Delta\gamma J), \quad \text{(A19)}$$

$$b = (D_0 - a(B_0 - \Delta\gamma B_1))/N, \quad \text{(A20)}$$

$$\chi^2 = a^2 A_0 + 2abB_0 - 2aC_0 + b^2 N - 2bD_0 + D_1. \quad \text{(A21)}$$

It is important to note that, as it stands, the measured values refer to a low-pass filtered version of the exponential current transient. It is, however, a fortuitous property of the exponential function that it remains exponential under a linear filtering process, as we prove in the equation below using a convolution to represent the filtering.

$$f(t + t_0) = \int K(t + t_0 - t')e^{-t'/\tau}\,dt' \quad \text{(A22)}$$

$$= e^{-t_0/\tau}\int K(t - t'')e^{-t''/\tau}\,dt'' \quad \text{(A23)}$$

$$= e^{-t_0/\tau} f(t). \quad \text{(A24)}$$

In these equations, $f(t)$ is the filtered version of the current $e^{-t'/\tau}$, whereas the filter is represented without loss of generality as the convolution kernel $K(t)$. Setting $t = 0$ gives the result that $f(t_0)$ is exponential with amplitude $f(0)$.

In addition to remaining exponential in time, the time constant $\tau$ and baseline $b$ are unchanged by the filtering process. The charge under the transient $q = a\tau$, in contrast, changes in a manner dependent on $\tau$, as can be seen by assuming the filtering kernel to be a Gaussian and performing the integration,

$$K(t) = (2\pi\sigma^2)^{1/2} e^{-(t-t_0)^2/2\sigma^2}, \quad \text{(A25)}$$

$$f(t) = e^{t_0/\tau + \sigma^2/2\tau^2} e^{-t/\tau}, \quad \text{(A26)}$$

where the parameter $t_0$ characterizes the time-delay of the filter and $\sigma$ characterizes the width. A correction can therefore be made by multiplying $q$ by $e^{f_1/\tau + f_2/\tau^2}$, where the constants $f_1$ and $f_2$ are determined empirically using the capacitance compensation controls on the EPC-7. Leaving the C-slow control fixed while varying the G-series control has the effect of varying $\tau$ while keeping the true $q$ constant. Any change in the measured $q$ is therefore due to filtering effects. By fitting $\log(q)$ versus $1/\tau$ with a polynomial, the constants $f_1$ and $f_2$ can therefore be determined and the measured $q$ corrected. Further details of the filtering kernel, which is not going to be precisely Gaussian, can be accommodated by generalizing the correction to a higher order polynomial in $1/\tau$, although, in practice, two terms proved to be sufficient.

This method therefore corrects the charge under the transient by extrapolating back to the beginning of an idealized unfiltered exponential transient. It proved to be relatively noisy in the case of a small cell capacitance, when the bulk of the current is in the rising phase of the transient that is ignored in the fit. A modification to the method corrects this problem, by integrating the current in the rising phase, adding the integrated current $q'$ back to the charge $q$ under the falling phase, as determined by the least-squares fit, and subtracting the charge included due to the baseline offset $\Delta b$ for the time from the voltage step (determined through the polynomial fit above) to the beginning of the exponential fit. Mathematically, this is expressed as

$$q \rightarrow q + q' - (f_1 + f_2/\tau)\Delta b. \quad \text{(A27)}$$

This modification extended the good noise performance of the method to small cells, but made the capacitance measurement sensitive to the pipette capacitance compensation control.

A further correction can be made because the apparent current transient actually includes the sum of all the lingering effects of previous current transients. The calculation is essentially the sum of a geometric series and results in the correction,

$$q \rightarrow q(1 + e^{-t_{period}/2\tau}), \quad \text{(A28)}$$

where $t_{period}$ is the period of the stimulus. The current transients are, however, sufficiently well spaced that this correction appears to be negligible.

The two sets of corrected exponential parameters can be averaged, and the membrane capacitance $C_m$, membrane conductance $G_m$, and access conductance $G_a$ calculated using the following equations

$$G_a = \frac{q/\tau + \Delta b}{\Delta v}, \quad \text{(A29)}$$

$$G_m = \frac{1}{\Delta v/\Delta b - 1/G_a}, \quad \text{(A30)}$$

$$C_m = \tau(G_a + G_m), \quad \text{(A31)}$$

where $\Delta v$ is the size of the voltage step and $\Delta b$ is the difference of the baselines between the first and second exponentials.

The use of capacitance compensation controls is often highly desirable in patch clamp experiments. The square wave method described above can be adapted relatively easily to use capacitance compensation, if the patch clamp amplifier provides computerized control settings (such as the EPC-9) or provides telegraph outputs indicating the current settings.

Because capacitance compensation essentially subtracts an exponential from the pipette current, it is necessary to add back the exponential in software prior to fitting the currents. The added exponential should reflect the filtering of the patch-clamp amplifier by adjusting the amplitude in a similar manner to that described above. If the conversion of the compensation settings (given as binary numbers or voltages) into circuit values (ohms and farads) is unknown; then this can be calibrated by recording $C_m$ and $G_a$ values with an open headstage as the compensation controls are adjusted.

R. Thompson was supported by National Institutes of Health (NIH) Traineeships in Molecular Biophysics GM08267 and in Pharmacology GM08210. Research by R.T. and W.W.W. in the Developmental Resource for Biophysical Imaging Opto-Electronics was supported by NIH-NCRR-

P41-RR04224 and NSF-BIR-8800278, and M.L. received support of NIH-R01-NS38200-01A2.

## REFERENCES

Albillos A., G. Dernick, H. Horstmann, W. Almers, G. Alvarez de Toledo, and M. Lindau. 1997. The exocytotic event in chromaffin cells revealed by patch amperometry. *Nature.* 389:509–512.

Barnett, D. W., and S. Misler. 1997. An optimized approach to membrane capacitance estimation using dual-frequency excitation. *Biophys. J.* 72: 1641–1658.

Breckenridge, L. J., and W. Almers. 1987. Final steps in exocytosis observed in a cell with giant secretory granules. *Proc. Natl. Acad. Sci. U.S.A.* 84:1945–1949.

Chen, P., and K. D. Gillis. 2000. The noise of membrane capacitance measurements in the whole-cell recording configuration. *Biophys. J.* 79:2162–70.

Clausen, C., and J. M. Fernandez. 1981. A low-cost method for rapid transfer function measurements with direct application to biological impedance analysis. *Pflugers Arch. Eur. J. Physiol.* 390:290–295.

Debus, K., J. Hartmann, G. Kilic, and M. Lindau. 1995. Influence of conductance changes on patch clamp capacitance measurements using a lock-in amplifier and limitations of the phase tracking technique. *Biophys. J.* 69:2808–2822.

De Matteis, M. A., G. DiTullio, R. Buccione, and A. Luini. 1991. Characterization of calcium-triggered secretion in permeabilized rat basophilic leukemia cells. *J. Biol. Chem.* 266:10452–10460.

Donnelly, D. F. 1994. A novel method for rapid measurement of membrane resistance, capacitance, and access resistance. *Biophys. J.* 66:873–877.

Fernandez, J. M., F. Bezanilla, and R. E. Taylor. 1982. Distribution and kinetics of membrane dielectric polarization. II. Frequency domain studies of gating currents. *J. Gen. Physiol.* 79:41–67.

Fernandez, J. M., E. Neher, and B. D. Gomperts. 1984. Capacitance measurements reveal stepwise fusion events in degranulating mast cells. *Nature.* 312:453–455.

Fidler, N., and J. M. Fernandez. 1989. Phase tracking: an improved phase detection technique for cell membrane capacitance measurements. *Biophys. J.* 56:1153–1162.

Fishman, H. M. 1985. Relaxations, fluctuations and ion transfer across membranes. *Prog. Biophys. Mol. Biol.* 46:127–162.

Gillis, K. D. 1995. Techniques for membrane capacitance measurements. *In* Single-Channel Recording, 2nd ed. B. Sakmann, and E. Neher (editors). Plenum Press, New York. 155–198.

Gillis, K. D. 2000. Admittance-based measurement of membrane capacitance using the EPC-9 patch-clamp amplifier. *Pflugers Arch. Eur. J. Physiol.* 439:655–664.

Hamill, O. P., A. Marty, E. Neher, B. Sakmann, and F. J. Sigworth. 1981. Improved patch-clamp technique for high-resolution current recording from cells and cell-free membrane patches. *Pflugers Arch. Eur. J. Physiol.* 391:85–100.

Joshi, C., and J. M. Fernandez. 1988. Capacitance measurements. An analysis of the phase detector technique used to study exocytosis and endocytosis. *Biophys. J.* 53:885–892.

Levis, R. A., and J. L. Rae. 1998. Low-noise patch-clamp techniques. *Methods Enzymol.* 293:218–266.

Lindau, M. 1991. Time-resolved capacitance measurements monitoring exocytosis in single cells. *Quart. Rev. Biophys.* 24:75–101.

Lindau, M., and E. Neher. 1988. Patch-clamp techniques for time-resolved capacitance measurements in single cells. *Pflugers Arch. Eur. J. Physiol.* 411:137–146.

Maiti, S., J. B. Shear, R. M. Williams, W. R. Zipfel, and W. W. Webb. 1997. Measuring serotonin distribution in live cells with three-photon excitation. *Science.* 275:530–532.

Neher, E. and A. Marty. 1982. Discrete changes of cell membrane capacitance observed under conditions of enhanced secretion in bovine adrenal chromaffin cells. *Proc. Natl. Acad. Sci. U.S.A.* 79:6712–6716.

Rohlicek, V., and J. Rohlicek. 1993. Measurement of membrane capacitance and resistance of single cells with two frequencies. *Physiol. Res.* 42:423–428.

Rohlicek, V., and A. Schmid. 1994. Dual-frequency method for synchronous measurement of cell capacitance, membrane conductance and access resistance on single cells. *Pflugers Arch. Eur. J. Physiol.* 428: 30–38.

Scepek, S., and M. Lindau. 1993. Focal exocytosis by eosinophils—compound exocytosis and cumulative fusion. *EMBO J.* 12:1811–1817.

Sigworth, F. J., H. Affolter, and E. Neher. 1995. Design of the EPC-9, a computer controlled patch clamp amplifier. 2. Software. *J. Neurosci. Methods.* 56:203–215.

Smith, C. B., and W. J. Betz. 1996. Simultaneous independent measurement of endocytosis and exocytosis. *Nature.* 380:531–534.

Spruce, A. E., L. J. Breckenridge, A. K. Lee, and W. Almers. 1990. Properties of the fusion pore that forms during exocytosis of a mast cell secretory vesicle. *Neuron.* 4:643–654.

Williams, R. M., J. B. Shear, W. R. Zipfel, S. Maiti, W. W. Webb. 1999. Mucosal mast cell secretion processes imaged using three-photon microscopy of 5-hydroxytryptamine autofluorescence. *Biophys. J.* 76: 1835–1846.